

Task-Driven Data Augmentation for Vision-Based Robotic Control

Shubhankar Agarwal¹ and Sandeep P. Chinchali¹

Abstract— Today’s robots often interface data-driven perception and planning models with classical model-based controllers. For example, drones often use computer vision models to estimate navigation waypoints that are tracked by model predictive control (MPC). Often, such learned perception/planning models produce erroneous waypoint predictions on out-of-distribution (OoD) or even adversarial visual inputs, which increase control cost. However, today’s methods to train robust perception models are largely task-agnostic – they augment a dataset using random image transformations or adversarial examples targeted at the vision model in *isolation*. As such, they often introduce pixel perturbations that are ultimately benign for control, while missing those that are most adversarial. In contrast to prior work that synthesizes adversarial examples for single-step vision tasks, our key contribution is to efficiently synthesize adversarial scenarios for multi-step, model-based control. To do so, we leverage differentiable MPC methods to calculate the sensitivity of a model-based controller to errors in state estimation, which in turn guides how we synthesize adversarial inputs. We show that *re-training* vision models on these adversarial datasets improves control performance on OoD test scenarios by up to 28.2% compared to standard task-agnostic data augmentation. Our system is tested on examples of robotic navigation and vision-based control of an autonomous air vehicle.

I. INTRODUCTION

Imagine a drone that must safely land on diverse moving targets using its on-board camera and a learned perception module, such as a deep neural network (DNN). The drone’s perception DNN, coupled with a downstream planning module, often outputs a sequence of waypoints that are tracked by MPC for a safe, low-cost trajectory [8], [10]. However, the drone will often operate in visual scenarios with radically different lighting, weather, and terrain conditions than its original training distribution. In this paper, we ask whether we can automatically synthesize adversarial visual scenarios for multi-step, *model-based* control tasks in order to re-train more robust robotic perception models.

Today’s methods to train robust perception models include data augmentation [9], [32], domain randomization [31], [30], and synthesis of adversarial examples for single-step vision tasks [15], [16], [35]. Collectively, these methods would add synthetic visual examples by randomly cropping, rotating, or altering the hue of pixels in a training distribution or adversarially altering them to affect perceptual predictions. However, we observe that such augmentation methods are largely *task-agnostic* and instead focus on improving vision models in isolation. As such, they often synthesize visual

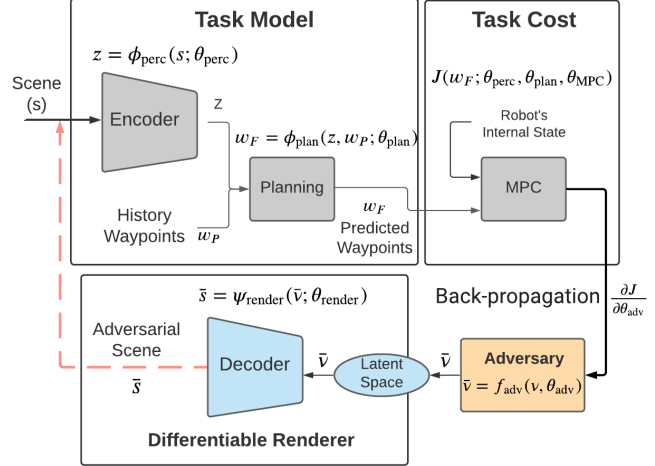


Fig. 1: **Differentiable Robot Learning Architecture:** A robot measures a visual scene s , which it maps through an encoder to yield scene embedding z . Given a history of waypoints w_p , a task module (planner) outputs a future set of waypoints w_F to track. Finally, these waypoints are tracked using a differentiable model predictive controller (MPC) that outputs a task cost J . We assume scenes s are rendered by a generative model, such as a differentiable renderer, that maps latent parameters describing a scene v to an image s . **Our key contribution** is to train an adversary (orange) to generate synthetic, but realistic, images \bar{s} that are poor for the current planner and controller. These scenes are then used to re-train the planning module for robust performance on OoD data.

examples that might be ultimately benign for control, while missing those that directly affect key state estimates.

Our work bridges recent advances in generative models [12], [28], differentiable rendering [25], [18], and differentiable MPC [5]. Collectively, these advances enable us to synthesize realistic visual scenes from a set of latent, often-interpretable, scene parameters and calculate their impact on control cost. Our principal contribution is a training procedure that efficiently perturbs the latent representation of a visual scene so that we render scenarios that are poor for control, but consistent with naturally-occurring data. Moreover, we can visualize the latent representations of visual scenes to understand how task-driven, adversarial data augmentation improves the quality and diversity of training examples. Finally, we show that re-training perception models on such adversarial scenes improves their generalization on unseen examples compared to today’s task-agnostic data augmentation methods.

Literature Review: Our work is broadly related to adversarial reinforcement learning (RL) in robotics, data augmentation, differentiable model predictive control (MPC), and differentiable rendering methods. We now highlight how our

¹ Department of Electrical and Computer Engineering (ECE), The University of Texas at Austin, Austin, TX {somi.agarwal, sandeepc}@utexas.edu

approach differs from related work.

It is well-known that many perception models are susceptible to adversarial examples [15], [6], [16], [35]. For example, techniques like the Fast Gradient Sign Method (FGSM) calculate the sensitivity of a pre-trained classifier to distortions in the image input, which guides how we synthesize small, human-imperceptible, pixel changes that cause misclassifications. However, to the best of our knowledge, there is very little work describing how such image perturbations ultimately affect *multi-step, model-based* control tasks (e.g., navigation) that rely on state estimates from deep models.

Our work is closest to, but distinct from, robust adversarial reinforcement learning (RARL) methods [22], [23], [26], [24]. First, these methods aim to improve a *control* policy, either by perturbing an agent’s dynamics or introducing an adversarial RL agent that physically impedes progress. In stark contrast, we focus on fixed, model-based control policies (often represented by a convex program), and instead focus on re-training perception models that provide state estimates that serve as input parameters for convex MPC. To do so, we leverage recent advances in differentiable MPC [5], [4], [7] to compute the sensitivity of the control cost to erroneous perceptual inputs. As such, we leverage the structure of the model-based controller to efficiently synthesize adversarial inputs as opposed to model-free RARL methods.

As noted earlier, today’s standard data augmentation for computer vision [32] is largely task-agnostic – random image crops or rotations might change perception waypoints in a way that barely affects control cost. Instead, our method leverages the structure of a model-based controller to targetedly perturb pixels that are most salient for control. The idea of task-driven data augmentation has already been applied to training graph neural networks (GNNs) by creating synthetic graphs with dropped nodes, edges etc. [36], [11]. However, our key distinction is that we compute the sensitivity of a multi-step control task to pixel perturbations and innovate new loss functions that promote rendering of realistic adversarial scenes. Finally, our work differs from gradient-free Bayesian Optimization [2] methods (e.g., for safety assurances for self-driving cars [33], [13]) since we explicitly leverage the gradient of MPC’s task cost.

Contributions: Given prior work, our contributions are:

- 1) First, we present a method to automatically synthesize adversarial examples for data-driven perception models that directly affect model-based control cost.
- 2) Second, we develop a novel loss function that flexibly trades-off the realism of adversarial examples with their impact on control cost by learning perturbations in a latent space that generates visual scenes.
- 3) Third, we show that re-training on these synthesized examples leads to better performance on unseen test data than today’s standard task-agnostic data augmentation. We demonstrate this result on a scenario where an aircraft must taxi on a runway using an on-board vision model in a photo-realistic simulator [1], [19].

Paper Organization: In Section II, we introduce how we integrate data-driven perception with differentiable MPC, and

present our algorithm for adversarial scenario generation in Section III. Then, in Section IV, we show strong experimental performance for our algorithm on challenging OoD scenarios. Finally, we conclude in Section V.

II. PROBLEM STATEMENT

We introduce our problem by describing the information flow in our differentiable robot learning architecture (Fig. 1).

Differentiable Perception and Planning Modules: The robot’s perception module $\phi_{\text{perception}}$ maps a high-dimensional visual observation s into a low-dimensional scene embedding z , denoted by:

$$z = \phi_{\text{perception}}(s; \theta_{\text{perc}}).$$

Here, θ_{perc} are parameters of the perception module, such as a DNN. Next, the robot must use the scene embedding z to plan a safe, collision-free trajectory to achieve its task. Often, we can represent a robot’s desired trajectory by a sequence of waypoints a robot should follow, such as a set of landmark poses in the xy plane a 2-D planar robot should follow. Then, the differentiable planning module maps scene embedding z and a vector of P past waypoints w_p to a vector of F future waypoints to follow, denoted by:

$$w_F = \phi_{\text{plan}}(z, w_p; \theta_{\text{plan}}).$$

Here, θ_{plan} are parameters of the differentiable planner. Henceforth, for brevity, we refer to the composition of the perception and planning modules as a task module $w_F = \phi_{\text{task}}(s, w_p; \theta_{\text{perc}}, \theta_{\text{plan}})$. In practice, the task module can be the cascaded operation of a perception and planning DNN.

Differentiable MPC: The next step is to control the robot to follow the waypoints w_F with minimal cost. Suppose the robot is at some initial state ζ_t and has a planning horizon of F steps. Then, its controller π should map the initial state ζ_t and future waypoints w_F into a sequence of controls from t to $t+F$, denoted by $u_{t:t+F} = \pi(\zeta_t, w_F; \theta_{\text{MPC}})$. Here, θ_{MPC} could represent feedback gains for MPC. Crucially, we define a task (control) cost $J(w_F; \theta_{\text{perc}}, \theta_{\text{plan}}, \theta_{\text{MPC}})$ which depends on the final waypoints the robot tracks w_F . Since the waypoints w_F depend on the previous perception and planning modules, the cost J implicitly depends on their parameters too. We give an example of an MPC task cost J in Sec. IV.

Differentiable Rendering Module: This paper analyzes how the ultimate MPC task cost J would increase if the robot observes an adversarial visual input \bar{s} instead of original image s . Henceforth, adversarial perturbations of any variable x are denoted \bar{x} . To do so, we need a process to generate, or render, realistic adversarial scenes \bar{s} . Fortunately, recent progress in generative models and differentiable rendering techniques in computer graphics makes rendering scenes \bar{s} possible [25], [27]. A differentiable renderer $s = \psi_{\text{render}}(v; \theta_{\text{render}})$ generates the robot’s scene s from latent parameters v that describe the scene and internal parameters θ_{render} of the rendering model. Often, the latent representation v of scene s could be interpretable and controllable, such as the mass, pose, lighting, and texture of different objects. Without loss of generality, the renderer in

our pipeline could also be a conventional generative model, such as the decoder in a Variational Autoencoder (VAE) [21] or a Generative Adversarial Network (GAN) [14]. All we require is a differentiable mapping that allows us to generate new scenes \bar{s} from latent parameters \bar{v} . Henceforth, we use the term differentiable renderer for ψ_{render} , even though we use VAE decoders since we rely on custom datasets without standard renderers.

End-to-End Differentiable Architecture: Since every aforementioned block in Fig. 1 is differentiable, we have an end-to-end differentiable mapping from scene parameters v to ultimate task cost J . Henceforth, we slightly re-define our notation for the task cost to be $J(v; \theta_{\text{perc}}, \theta_{\text{plan}}, \theta_{\text{MPC}})$ to make it explicit that the cost depends on the latent scene representation v . This is because v generates scene s , which is mapped to MPC waypoints w_F through the task module. As such, we can back-propagate the gradient of the MPC task cost J with respect to scene parameters v to efficiently search for adversarial scene parameters \bar{v} .

Training and Test Datasets: To formally define our problem statement, we must first formalize our dataset notation. A dataset contains N tuples of inputs x and ground-truth labels y denoted by $\mathcal{D} = \{x, y\}_{i=1}^N$. Specifically, each example $x = (s, v, w_p)$ represents the robot's scene input s , corresponding latent representation v from the renderer, and waypoint history w_p . From these, the task model predicts a ground-truth target vector $y = w_F$ of future robot waypoints. In practice, these labels can come from an oracle planner to emulate, such as a Frenet Planner, that has perfect access to ground-truth scenes s and waypoints w_p, w_F .

Henceforth, the subscript b in the dataset notation \mathcal{D}_b will represent the type of dataset, such as whether it is an original image, from data augmentation, or adversarial training. Likewise, the superscript a will represent if the dataset is from the *train* or *test* distribution. For example, the original training and test datasets are given by $\mathcal{D}_{\text{orig}}^{\text{train}}$ and $\mathcal{D}_{\text{orig}}^{\text{test}}$. Likewise, a held-out OoD test dataset is denoted by $\mathcal{D}_{\text{OoD}}^{\text{test}}$. Crucially, we define a training function TRAIN that uses supervised learning to train the task model to output correct waypoints w_F given the scene s . The notation $\theta_{\text{perc}}^0, \theta_{\text{plan}}^0 \leftarrow \text{TRAIN}(\mathcal{D}_{\text{orig}}^{\text{train}})$ indicates we train the nominal task model parameters on the original training dataset.

For a focused contribution, we consider a practical scenario where the robot has an MPC controller with fixed parameters θ_{MPC} . Moreover, we have already pre-trained a nominal task model $\theta_{\text{perc}}^0, \theta_{\text{plan}}^0$ on original images in $\mathcal{D}_{\text{orig}}^{\text{train}}$. Given these inputs, our problem is generate an additional dataset $\mathcal{D}_{\text{new}} = \{x, y\}_{i=1}^M$ of M datapoints such that re-training the perception and planning models on combined dataset $\mathcal{D}_{\text{orig}}^{\text{train}} \cup \mathcal{D}_{\text{new}}$ will minimize task cost J on a held-out OoD test dataset $\mathcal{D}^{\text{test}}$. We only consider adding M extra examples to limit training costs. Formally, our problem becomes:

Problem 1 (Data Augmentation for Control Tasks): Given fixed MPC parameters θ_{MPC} , original training dataset $\mathcal{D}_{\text{orig}}^{\text{train}}$, and unseen held-out test dataset $\mathcal{D}^{\text{test}}$, find a new

dataset $\mathcal{D}_{\text{new}} = \{x, y\}_{i=1}^M$ of size M such that:

$$\theta_{\text{perc}}^*, \theta_{\text{plan}}^* = \arg \min_{\theta_{\text{perc}}, \theta_{\text{plan}}} \mathbb{E}_{(s', v', w_p, w_F') \sim \mathcal{D}^{\text{test}}} J(v'; \theta_{\text{perc}}, \theta_{\text{plan}}, \theta_{\text{MPC}}),$$

where $\theta_{\text{plan}}^*, \theta_{\text{perc}}^* \leftarrow \text{TRAIN}(\mathcal{D}_{\text{orig}}^{\text{train}} \cup \mathcal{D}_{\text{new}})$.

It is hard to analytically find the best additional dataset of M points to minimize task cost on OoD data. This is because practical task models require training non-convex DNNs and the test dataset $\mathcal{D}^{\text{test}}$ is a-priori unknown. We now describe our adversarial dataset generation approach for control tasks.

III. ADVERSARIAL SCENARIO GENERATION ALGORITHM

We hypothesize that we can generate a dataset of adversarial scenarios \mathcal{D}_{adv} where the original task model performs poorly. Then, by re-training the task model on the joint dataset $\mathcal{D}_{\text{orig}}^{\text{train}} \cup \mathcal{D}_{\text{adv}}$, we hope to improve its robust generalization. To do so, we introduce a differentiable adversary to generate the new dataset \mathcal{D}_{adv} , shown in orange in Fig. 1. The adversary maps the original latent scene representation v to a perturbed representation $\bar{v} = f_{\text{adv}}(v; \theta_{\text{adv}})$, where θ_{adv} are trainable parameters. Our goal is to train the parameters such that the adversarial scene representation \bar{v} increases the task cost J compared to the original scene representation v .

Adversary Loss Function: We now introduce a novel loss function to train the adversary f_{adv} . Intuitively, the adversary's loss function must perturb the latent scene representation v to \bar{v} such that the task cost increases. At the same time, it must ensure that the new rendered scene from \bar{v} is realistic and fairly close to v . This is necessary since we want to augment our training dataset with scenes represented by \bar{v} that a robot can plausibly encounter during real-world test deployment. Therefore, the following adversarial loss function must delicately balance the differentiable task cost and distance loss between \bar{v} and v .

Adversarial Task Cost: Given an original latent representation v of the scene, we invoke the adversary to generate the adversarial latent representation by $\bar{v} = f_{\text{adv}}(v; \theta_{\text{adv}})$. Then, we simply invoke the end-to-end differentiable modules in Fig. 1. Importantly, we use the pre-trained task module parameters $\theta_{\text{perc}}^0, \theta_{\text{plan}}^0$ since they will only be re-trained after the adversarial dataset generation procedure. Specifically, the renderer first generates a new perturbed visual scene $\bar{s} = \psi_{\text{render}}(\bar{v}; \theta_{\text{render}})$. Next, the task model outputs a new waypoint prediction $\bar{w}_F = \phi_{\text{task}}(\bar{s}, w_p; \theta_{\text{perc}}^0, \theta_{\text{plan}}^0)$. Finally, we calculate the new task cost $J(\bar{v}; \theta_{\text{perc}}^0, \theta_{\text{plan}}^0, \theta_{\text{MPC}}, \theta_{\text{adv}})$. Importantly, we note that the task cost J implicitly depends on the adversary parameters θ_{adv} since they generate perturbed scene representation \bar{v} . For a concise notation, we will represent the task cost $J(\bar{v}; \theta_{\text{perc}}^0, \theta_{\text{plan}}^0, \theta_{\text{MPC}}, \theta_{\text{adv}})$ as $J(\bar{v}; \theta_{\text{adv}})$, since the parameters $\theta_{\text{perc}}^0, \theta_{\text{plan}}^0, \theta_{\text{MPC}}$ are fixed and \bar{v} depends on the adversary parameters θ_{adv} .

Consistency (Distance) Loss: To promote generation of plausible adversarial images, we introduce a consistency loss $I(v, \bar{v}) \in \mathbb{R}$. Calculating the distance loss in the *latent space* is a novelty of our loss function based on the observation that similar scenes s and \bar{s} might be very far in the high-dimensional image space but might be close in the latent

space of the renderer ψ_{render} . Moreover, if the latent space parameters v have *physical meaning*, such as the mass, positions, and colors of key objects in the scene, we can interpret the distance in the v space. In our experiments, we use the L_2 norm distance between latent space variables \bar{v} and v , although our general method can accommodate other differentiable distance loss functions.

Overall Adversarial Loss Function: Finally, our adversarial loss function allows us to trade-off extra control cost while incentivizing realism of the rendered synthetic scene. During adversarial scenario generation, only the adversary's parameters θ_{adv} are trained while the initial task module parameters are kept fixed. The loss function is:

$$\mathcal{L}(v, \bar{v}; \theta_{\text{adv}}) = J(\bar{v}; \theta_{\text{adv}}) - \kappa I(v, \bar{v}). \quad (1)$$

Here, the distance loss is weighted by κ in the loss function, which can be flexibly set by a roboticist depending on how adversarial they prefer rendered scenarios to be.

Adversary Training: Algorithm 1 shows our complete adversarial training procedure. The inputs are an original training dataset $\mathcal{D}_{\text{orig}}^{\text{train}}$, fixed MPC parameters θ_{MPC} , and pre-trained task module parameters $\theta_{\text{perc}}^0, \theta_{\text{plan}}^0$. We iterate over each point in the training dataset and generate its corresponding adversarial example by performing gradient ascent on our adversarial loss function (Eq. 1). Then, we save the most adversarial synthetic examples generated by trainable adversary f_{adv} for subsequent data augmentation. To do so, we use a new adversary for each datapoint rather than training a common adversary for the whole dataset.

Starting from line 3, we iterate through the original dataset $\mathcal{D}_{\text{orig}}^{\text{train}}$. Each datapoint x_i is a tuple of input scene s_i , corresponding renderer latent representation v_i , and past waypoints w_p . Lines 4-7 describe how we initialize a *new trainable* adversary for each datapoint. First, we obtain the latent space representation v_i of the datapoint x_i from the differentiable renderer ψ_{render} . In line 4, we initialize a new adversary f_{adv} with random weights $\theta_{\text{adv}}^{k=0}$, which will be specific to the datapoint x_i . Since we train the adversary parameters for K gradient descent steps, we use superscript k to indicate the adversary's parameters at training step k . Likewise, we index the new adversarially-generated latent representation at each step k by \bar{v}^k . Finally, in lines 5-7, we initialize a tuple (\bar{x}, \bar{y}) that will indicate the adversarially generated datapoint and label. They are initialized to the *original* training dataset's values.

The crux of our algorithm is in lines 8-19, where we perform K gradient update steps to train the adversary f_{adv} . In each gradient step k , we update the adversary parameters to θ_{adv}^k using adversarial loss function L and back-propagation (lines 9-14). In lines 15-19, we store the adversarial tuple (\bar{x}^k, y_i) if it has higher task cost J than the previous best task cost J^* . Finally, after K gradient steps, we append the best adversarial datapoint (\bar{x}, \bar{y}) to dataset \mathcal{D}_{adv} in line 21. Crucially, we keep all the network weights frozen during adversarial training, and only adversary parameters θ_{adv} are updated. At the end, we have generated a new adversarial dataset, which is augmented with the original dataset to retrain the task model to yield new parameters $\theta'_{\text{perc}}, \theta'_{\text{plan}}$ on

```

1 Input:  $\theta_{\text{perc}}^0, \theta_{\text{plan}}^0, \theta_{\text{MPC}}, \mathcal{D}_{\text{orig}}^{\text{train}}$ 
2 Initialize empty new adversarial dataset  $\mathcal{D}_{\text{adv}} = \{\}$ 
3 for  $(x_i = \{s_i, v_i, w_p\}, y_i) \leftarrow \mathcal{D}_{\text{orig}}^{\text{train}}, 0 \leq i \leq N$  do
4   Init. adver  $f_{\text{adv}}(v_i; \theta_{\text{adv}}^{k=0})$  with random  $\theta_{\text{adv}}^{k=0}$ 
5   Init. adversarial latent rep.  $\bar{v}^{k=0} = v_i$ 
6   Best Task Loss  $J^* = -\infty$ 
7   Init. Adv. Tuple  $(\bar{x}, \bar{y}) = (x_i, y_i)$ 
8   for  $k \leftarrow 1$  to  $K$  do
9     Get adv. latent params  $\bar{v}^k = f_{\text{adv}}(\bar{v}^{k-1}; \theta_{\text{adv}}^{k-1})$ 
10    Render scene  $\bar{s}^k = \psi_{\text{render}}(\bar{v}^k; \theta_{\text{render}})$ 
11    Get waypoints  $\bar{w}_F^k = \phi_{\text{task}}(\bar{s}^k, w_p; \theta_{\text{perc}}^0, \theta_{\text{plan}}^0)$ 
12    Calculate task cost  $J(\bar{v}^k; \theta_{\text{adv}}^{k-1})$ 
13    Calc. Loss  $L = \mathcal{L}(v_i, \bar{v}^k; \theta_{\text{adv}}^{k-1})$ 
14     $\theta_{\text{adv}}^k \leftarrow \text{BACKPROP}(\theta_{\text{adv}}^{k-1}, L)$ 
15    if  $J(\bar{v}^k, \theta_{\text{adv}}^{k-1}) \geq J^*$  then
16      Update most adv. scene  $\bar{x}^k = \{\bar{s}^k, \bar{v}^k, w_p\}$ 
17      Update adv. example  $(\bar{x}, \bar{y}) = (\bar{x}^k, y_i)$ 
18       $J^* \leftarrow J$ 
19    end
20  end
21  Append adv. example  $(\bar{x}, \bar{y})$  to  $\mathcal{D}_{\text{adv}}$ 
22 end
23 Return:  $\theta'_{\text{perc}}, \theta'_{\text{plan}} \leftarrow \text{TRAIN}(\mathcal{D}_{\text{orig}}^{\text{train}} \cup \mathcal{D}_{\text{adv}})$ 

```

Algorithm 1: Adversary Training

line 23. We now experimentally show the benefits of our task-driven data augmentation approach.

IV. EXPERIMENTAL RESULTS

We now evaluate our method (Algorithm 1) on two diverse tasks. The first task is a simple, but illustrative, toy example of robotic motion planning. In the second experiment, an autonomous aircraft must taxi by tracking a runway centerline based on visual inputs in challenging weather conditions.

A. Experiment Preliminaries

Adversary Model: We use a linear model for our adversary $f_{\text{adv}}(v; \theta_{\text{adv}}) = \theta_{\text{adv}} v$, where $\theta_{\text{adv}} \in \mathbb{R}^{n \times n}$. Our subsequent experiments show that a linear adversary is expressive enough to generate realistic scenarios that are poor for control tasks. Our method allows for more complex neural network adversary models since it is fully differentiable.

Distance Loss and Regularization: We use the mean squared error (MSE) as the consistency loss $I(v, \bar{v}) = \|\bar{v} - v\|_2^2$ in Eq. (1). This ensures that the adversarial scene's latent representation does not deviate too far from that of the original. Since the full pipeline in Fig. 1 is differentiable, we can easily train the adversary by computing the gradient of the loss L with respect to the adversary's parameters θ_{adv} using automatic differentiation libraries. Finally, as shown in the experiments, the consistency loss weight κ can be flexibly set by the user based on how adversarial they want synthetic examples to be.

Variational Autoencoder (VAE): We use a VAE [21] as the differentiable rendering module ψ_{render} from Section II.

VAEs have gained significant popularity because of their more stable training procedures compared to Generative Adversarial Networks (GANs). It is important to note that we only use the VAE *Decoder* as the differentiable rendering module, which takes parameters v as input and outputs the image s of the scene. We keep the *Decoder* frozen after training it initially on the whole training dataset.

Differentiable Model Predictive Control (MPC): In both the tasks, we will formulate the task cost $J(w_F)$ for an MPC problem with quadratic costs and linear constraints, as shown in Eq. 2. The planning module provides the MPC controller with a waypoint vector w_F for F future timesteps to track. The robot's state at discrete time t is denoted by $\zeta_t \in \mathbb{R}^{4 \times 1}$, defined as $\zeta_t = \{l_x, l_y, v, \theta\}$ for both experiments. Here, l_x and l_y are the robot's x, y location in meters, v is the speed in meters/sec, and θ is the robot's heading angle in radians. The robot's control input at time t is defined as $u_t = \{a, \gamma\}$, where a is the robot's acceleration in m/s^2 and γ is the robot's steering input in radians/sec.

Our main goal is to formulate the task cost $J(w_F)$, which is a standard quadratic cost penalizing state deviations and control effort. Namely, $\mathbf{Q} \in \mathbb{R}^{4 \times 4}$ is the state cost matrix and $\mathbf{R} \in \mathbb{R}^{2 \times 2}$ is the control cost matrix. The matrices $\mathbf{A} \in \mathbb{R}^{4 \times 4}$ and $\mathbf{B} \in \mathbb{R}^{4 \times 2}$ define the robot's dynamics. For the first experiment, we use standard double integrator dynamics while the second experiment uses linearized unicycle dynamics. The robot has box control constraints $u_{\min} \leq u_t \leq u_{\max}$ bounding the minimum and maximum acceleration and steering angle. Likewise, box state constraints $\zeta_{\min} \leq \zeta_t \leq \zeta_{\max}$ define limits on the velocity and linear obstacle avoidance constraints. These constraints, used only in our first motion planning example, were calculated by drawing perpendicular hyperplanes from the obstacles. Given a set of F future waypoints $w_F = \{w_0, w_1, \dots, w_{F-1}\}$ for a planning horizon starting at $t = 0$, our MPC task cost and problem become:

$$\begin{aligned} \min_{\zeta_{0:F}, u_{0:F-1}} \quad & J(w_F) = \sum_{t=0}^F (w_t^\top - \zeta_t^\top) \mathbf{Q} (w_t - \zeta_t) + \sum_{t=0}^{F-1} u_t^\top \mathbf{R} u_t \\ \text{such that} \quad & \zeta_{t+1} = \mathbf{A} \zeta_t + \mathbf{B} u_t \\ & u_{\min} \leq u_t \leq u_{\max} \\ & \zeta_{\min} \leq \zeta_t \leq \zeta_{\max}. \end{aligned} \quad (2)$$

Our key step is to calculate the sensitivity of the task cost J to adversarial perturbations in the image s in order to train the adversary. To do so, we use advances in differentiable MPC to calculate the gradient of MPC's solution and task cost (a convex program) with respect to its problem parameters (i.e., waypoint predictions w_F). Then, we back-propagate through the differentiable pipeline in Fig. 1 to compute the gradient of MPC's task cost with respect to the adversary's parameters. Both experiments use the CVXPYLAYERS Pytorch library for differentiable convex programs [3].

Architectures: Both experiments use DNNs for all modules in Fig. 1 except model-based control. The perception module $\phi_{\text{perception}}$ is a convolutional VAE *Encoder* since it must map image s to an embedding z that can be used by the planner.

For the planner, we achieved success with both simple multi-layer perceptrons (MLPs) and CNNs. Our algorithm is agnostic to the type of deep network since it aims to improve any general, differentiable task model. Further details about model and training parameters are provided in Appendix A.

B. Datasets and Benchmark Algorithms

Recall the dataset notation from Section II. We compare task models trained on the following different datasets:

- 1) **ORIGINAL:** The task model (i.e., both perception and planning models) is *only* trained on the original $\mathcal{D}_{\text{orig}}^{\text{train}}$.
- 2) **DATA ADDED:** We add more training examples from the same (or very similar) distribution as the original training dataset, denoted by $\mathcal{D}_{\text{add}}^{\text{train}}$. This tests whether more examples are necessary to achieve better performance. The task model is then trained on the union of the original and added dataset, denoted by $\mathcal{D}_{\text{add}}^{\text{train}} \cup \mathcal{D}_{\text{orig}}^{\text{train}}$.
- 3) **DATA AUGMENTATION:** We apply standard *task-agnostic* data augmentation to the original training data. For the case of image inputs, we applied random contrast, random brightness and random blur to the images s . We refer to this widely-used scheme as *task-agnostic* as it solely aims to improve the perception model without accounting for the MPC task. The augmented dataset is denoted by $\mathcal{D}_{\text{aug}}^{\text{train}}$ and we re-train the task model on $\mathcal{D}_{\text{aug}}^{\text{train}} \cup \mathcal{D}_{\text{orig}}^{\text{train}}$.
- 4) **TASK DRIVEN (Ours):** We use Algorithm 1 to synthesize adversarial dataset $\mathcal{D}_{\text{adv}}^{\text{train}}$. Then, we *re-train* the task model on $\mathcal{D}_{\text{adv}}^{\text{train}} \cup \mathcal{D}_{\text{orig}}^{\text{train}}$.

Test Datasets: We test all the above training schemes on several independent, held out test datasets. First, we report the accuracy on the original dataset's test images $\mathcal{D}_{\text{orig}}^{\text{test}}$. Next, we report on OoD dataset $\mathcal{D}_{\text{OoD}}^{\text{test}}$, such as different weather conditions from the training distribution. Then, to confirm the rendered scenarios are indeed adversarial, we also report performance on the adversarially perturbed versions of the original test dataset $\mathcal{D}_{\text{adv}}^{\text{test}}$, which are generated by Alg. 1.

C. Illustrative Toy Example: 2D Obstacle Avoidance.

We now introduce a simple task where a planar 2-D robot has to navigate around obstacles to reach a goal location, as pictured in Fig. 3. This experiment demonstrates how adversarial training creates more challenging scenarios for the task model to plan in. Furthermore, we quantitatively show that a task model trained on adversarial scenarios $\mathcal{D}_{\text{adv}}^{\text{train}}$ learns to avoid collisions more successfully and with lower control cost compared to standard training procedures.

The input to the 2-D planar robot is a 100×100 grey-scale image s of the scene, including obstacles and the goal g , indicated by a star-shaped marker. Given the sensory input s , the task model $w_F = \phi_{\text{task}}(s, w_P)$ is a perception-planning module that outputs a sequence of future waypoints w_F for the robot to navigate. A waypoint w_F is simply a pose the robot must move to in the xy plane. The task model ϕ_{task} uses a history of past waypoints w_P to improve its predictions. The linear MPC task cost is defined in Eq. 2.

We synthetically created the training $\mathcal{D}_{\text{orig}}^{\text{train}}$ and the held-out test datasets $\mathcal{D}_{\text{orig}}^{\text{test}}$ and $\mathcal{D}_{\text{OoD}}^{\text{test}}$ for the experiments. As

Fig. 2: Our method improves collision avoidance on challenging motion planning environments: We show the number of collisions with an obstacle for different training schemes on the original, OoD, and synthetic adversarial test environments. A single collision occurs when the MPC-enacted trajectory intersects an ellipsoidal obstacle. The columns represent how many scenarios of the 2200 test scenarios had even a single collision for held-out test datasets $\mathcal{D}_{\text{orig}}^{\text{test}}$, $\mathcal{D}_{\text{OoD}}^{\text{test}}$ and $\mathcal{D}_{\text{adv}}^{\text{test}}$ respectively. The best performance is bolded and rows correspond to benchmark schemes.

Algorithm	$\mathcal{D}_{\text{orig}}^{\text{test}}$	$\mathcal{D}_{\text{OoD}}^{\text{test}}$	$\mathcal{D}_{\text{adv}}^{\text{test}}$
ORIGINAL	389	585	1058
DATA-ADDED	314	552	1044
DATA AUGMENT	321	489	933
TASK-DRIVEN (OURS)	334	422	623

shown in Fig. 3, each scenario had randomly generated ellipsoid obstacles with random sizes and locations. The ground truth waypoints $y = w_F$ are generated using a standard Frenet Planner [34] that has full access to all obstacles and start/goal locations for the entire scene. The synthetic dataset contained $|\mathcal{D}_{\text{orig}}^{\text{train}}| = 7000$ training scenarios and $|\mathcal{D}_{\text{orig}}^{\text{test}}| = 2200$ test scenarios. A larger similar dataset had $|\mathcal{D}_{\text{add}}^{\text{train}}| = 10000$ training examples. Another dataset of $|\mathcal{D}_{\text{aug}}^{\text{train}}| = 10000$ training examples was generated from task-agnostic data augmentation. The synthetic adversarial dataset generated by our method had $|\mathcal{D}_{\text{adv}}^{\text{train}}| = 10000$ training scenarios and $|\mathcal{D}_{\text{adv}}^{\text{test}}| = 2200$ adversarial test scenarios. We used $K = 10$ gradient steps in Algorithm 1 to generate the adversarial scenarios. Finally, we also generated a challenging OoD test dataset, $\mathcal{D}_{\text{OoD}}^{\text{test}}$, where the ellipsoid obstacles were samples from a different distribution than the original dataset $\mathcal{D}_{\text{orig}}^{\text{train}}$. Specifically, ellipsoid obstacles were bigger and closer in the OoD test dataset, thus making it hard for the robot to plan. We use a history of $P = 10$ past waypoints to predict the next $F = 20$ future waypoints.

The experiment shows that training the task model with additional adversarial data using Alg. 1 leads to superior performance compared to all benchmarks described in Sec. IV-B. We quantitatively compare the performance of all benchmarks on the number of collisions with obstacles, the average task cost J , and the mean-squared error (MSE) in predicting the waypoints on all test datasets. Finally, we qualitatively show that our rendered scenarios are adversarial and realistic compared to the training distribution.

Quantitative results: Table 2 shows the number of scenarios with collisions for all training schemes. Our TASK DRIVEN approach was able to perform as well as the DATA AUGMENTATION, DATA ADDED, and ORIGINAL benchmarks on the original test dataset. Additionally, the TASK DRIVEN approach significantly outperformed the DATA AUGMENTATION scheme by 49%, DATA ADDED scheme by 67% and ORIGINAL scheme by 69% on the adversarial test dataset $\mathcal{D}_{\text{adv}}^{\text{test}}$. Furthermore, our TASK DRIVEN approach outperformed the DATA AUGMENTATION scheme by 15.8%, DATA ADDED scheme by 30.8% and ORIGINAL scheme by 38.6% on the unseen OoD test dataset $\mathcal{D}_{\text{OoD}}^{\text{test}}$. Thus, our training scheme TASK-DRIVEN leads to significantly fewer

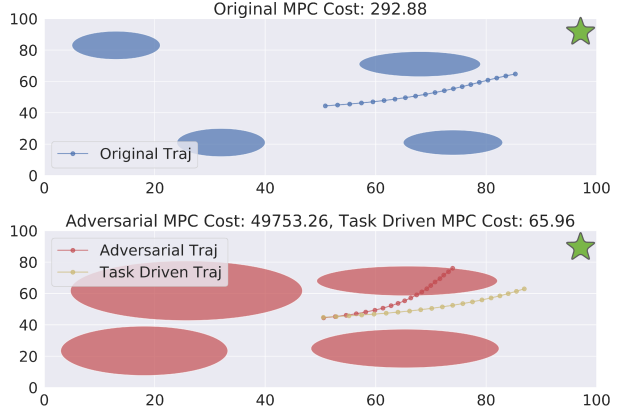


Fig. 3: Our method’s Synthesized Adversarial Scenarios: The robot’s goal is to navigate from a start location at $(0,0)$ to the goal at $(100,100)$ (green star). Original Scene (Top): The blue obstacles (4 ellipsoids) represent the original scene. Adversarial Scene (Bottom): The red obstacles in the bottom are adversarially created using our method for the original scenario above it. The waypoint trajectories (small sequential dots) are generated by the task model for the corresponding scene, and MPC task cost is given in the title. Clearly, the adversarial scenario generates much higher MPC costs by moving the obstacles in the robot’s intended path. Crucially, the waypoint trajectory generated by our *re-trained* TASK DRIVEN scheme (yellow) learns to better avoid the obstacles with lower MPC cost. Fig. 8 shows additional examples.

collisions on challenging OoD scenarios.

We now illustrate that our scheme also reduces the MPC task cost J . Fig. 4 (top left) shows the MPC task cost for all training schemes on 2200 held-out test datasets. On the original test dataset, our TASK-DRIVEN scheme (red) performs on par with the ORIGINAL (blue) scheme and slightly worse than the DATA-ADDED (orange) and DATA AUGMENTATION (green) schemes. The DATA-ADDED scheme’s performance is expected because it is trained on more original data than our TASK-DRIVEN scheme, which allows it to perform slightly better on the original test dataset. However, the key benefits of our approach are shown on the synthetic adversarial test dataset and held-out OoD dataset. The key take-away is that our scheme significantly outperforms the DATA AUGMENTATION scheme, with 204% less average MPC cost (Wilcoxon p-value of 0.0) on the synthetic adversarial test dataset and 80% less average MPC cost (Wilcoxon p-value of 0.0) on the held-out OoD dataset.

We now illustrate why our method is able to reduce the ultimate task cost. Specifically, Fig. 4 (top right) shows that our TASK-DRIVEN scheme achieves lower MSE for predicting ground-truth waypoints from the Frenet Planner than competing benchmarks. While all methods perform similarly on the original test dataset, the key gains of our scheme are on the adversarial test dataset and held-out OoD dataset. Our scheme significantly outperforms standard data augmentation by achieving 264.5% less average waypoint MSE on the synthetic adversarial test dataset and 4.5% less average waypoint MSE on the held-out OoD dataset.

Qualitative Results: Fig. 3 shows a challenging adversarial scenario that is automatically synthesized by our method

Toy Examples: 2D Obstacle Avoidance

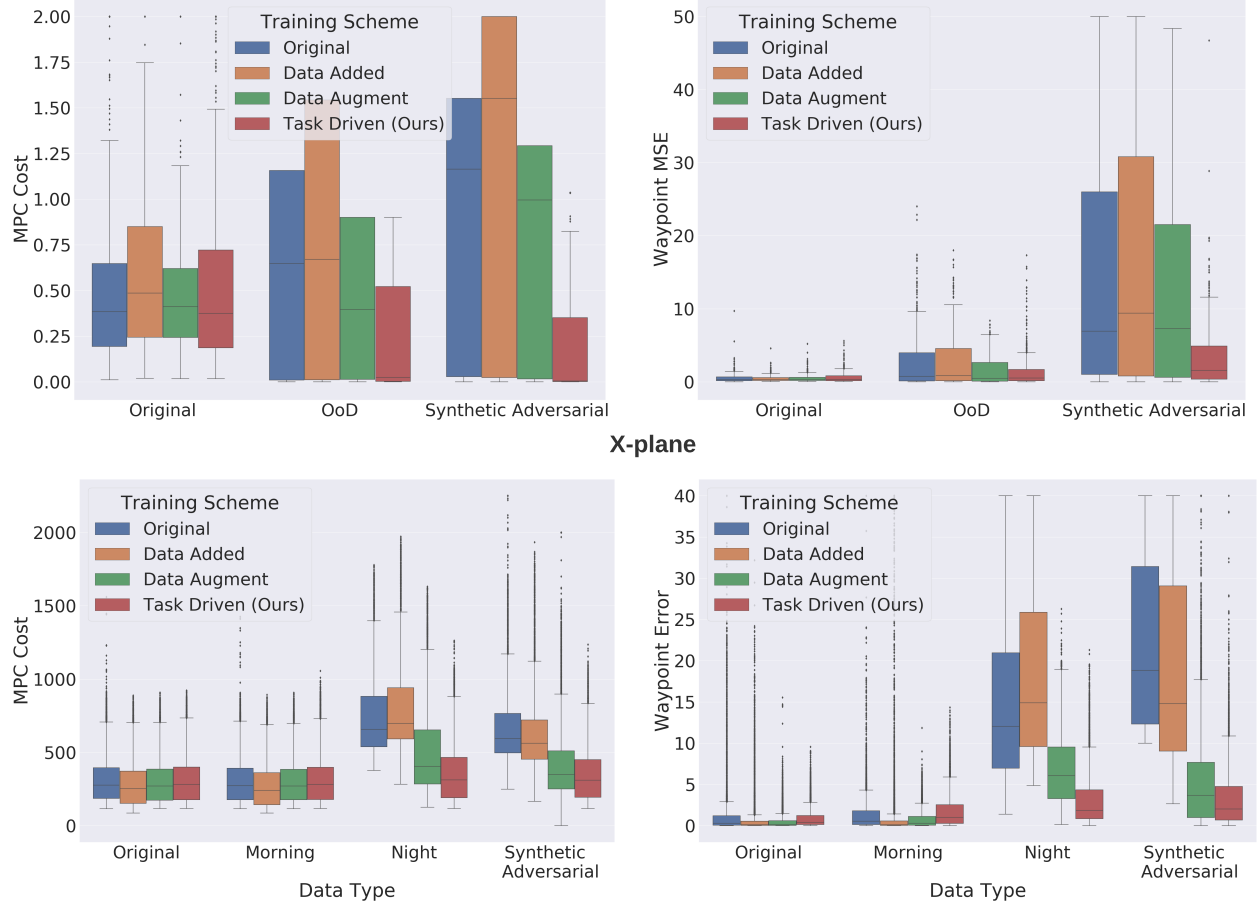


Fig. 4: **Benefits of Task-Driven Data Augmentation for Simple Motion Planning and X-Plane Dataset:** We show the MPC task cost J (left) and MSE for waypoint predictions (right) for the ORIGINAL (blue), DATA ADDED (yellow), DATA AUGMENTATION (green) and TASK DRIVEN (red) training schemes on held-out test environments. The x-axis shows different test conditions, and lower task cost and waypoint MSE (y-axis) are better. Our TASK DRIVEN scheme (red) works on par with other task models on the *Original* test data for both metrics and experiments. However, it significantly outperforms other task models on challenging scenarios in the *out-of-distribution* (*OoD*) dataset (*Night* images for X-Plane), and *Synthetic Adversarial* test datasets. Crucially, our TASK DRIVEN scheme (red) is able to generalize much better to the OoD dataset compared to all other training schemes. We beat today’s method of task-agnostic data augmentation (green) which often applies image augmentations that are ultimately benign for MPC. The DATA ADDED training scheme has high variance on OoD and Synthetic Adversarial datasets since it overfits to the Original dataset.

in dataset $\mathcal{D}_{\text{adv}}^{\text{train}}$. Our training scheme brings obstacles closer to the robot’s originally intended waypoints and path, making it harder to find a collision-free path. Naturally, this increases the task cost since the robot has to make wider turns and swerves. Therefore, rather than augmenting our dataset with well-understood scenarios already reflected in the training distribution, our scheme targetedly adds challenging scenarios that make the model more robust.

D. X-plane: Autonomous Vision-Based Airplane Taxiing

We now test our method on an autonomous aircraft taxiing problem. As shown in Fig. 5, the airplane has a wing-mounted camera and passes the images through a perception model to estimate its distance and heading angle relative to the center-line of a runway. Then, it uses differentiable MPC to navigate to the runway center-line with minimal control

cost. We use a public dataset from the photo-realistic X-Plane simulator [1] consisting of images from the plane’s wing-mounted camera in diverse weather conditions and at various poses on the runway. This standard benchmark dataset has been used in recent works on robust and verified perception [19], [29], [20]. Our prime goal is to test that our adversarial training method yields models that outperform benchmarks at generalizing to challenging OoD weather conditions.

1) *Setting:* The input to our “robot” is a 128×128 RGB image s of the runway taken from the right wing. The task model $w_F = \phi_{\text{task}}(s, w_P)$ is a perception-planning module that outputs the desired pose of the airplane w_F , given this sensory input s and a history of waypoints w_P . Specifically, the task model outputs a single waypoint w_F , which is a tuple of the distance to the centerline of runway c and the heading angle θ , denoted by $w_F = (c_i, \theta_i)_{i=0}^F$ for $F = 1$.

$w_P = (c_i, \theta_i)_{i=0}^P$ is a history of the $P = 10$ past waypoints which are used to improve the planning model’s predictions. MPC with linearized dynamics (Eq. 2) is used to plan a sequence of controls to navigate to the center-line.

Images from Diverse Weather Conditions: We will represent the whole X-plane dataset as $\Gamma = \{\mathcal{D}_{\text{afternoon}}, \mathcal{D}_{\text{morning}}, \mathcal{D}_{\text{overcast}}, \mathcal{D}_{\text{night}}\}$, where each dataset corresponds to the subscripted weather condition. Each individual weather dataset in Γ has 44,000 training scenarios and 11,000 testing scenarios. Ground truth waypoints are obtained from the X-Plane simulator.

Our goal is to establish that we can re-train a perception model that robustly generalizes (with good control performance) to OoD weather conditions. To do so, we start with a perception model that is *initially* only trained on afternoon conditions and evaluate its performance on held-out test images across OoD weather conditions. To do so, we will compare 4 different task models ϕ_{task} . The ORIGINAL model is only trained on $\mathcal{D}_{\text{afternoon}}^{\text{train}}$, while the DATA ADDED model is trained on $\mathcal{D}_{\text{add}}^{\text{train}} = \mathcal{D}_{\text{afternoon}}^{\text{train}} \cup \mathcal{D}_{\text{morning}}^{\text{train}}$ since the morning and afternoon are visually similar.

Today’s standard benchmark of task-agnostic data augmentation is trained on $\mathcal{D}_{\text{train}}^{\text{aug}} = \mathcal{D}_{\text{afternoon}}^{\text{train}} \cup \mathcal{D}_{\text{aug}}^{\text{train}}$, where we perform image augmentations (random crops, rotations, and hue alterations) on the original afternoon training data using the open-source Albumentations library [9]. Finally, our TASK DRIVEN model is trained on $\mathcal{D}_{\text{afternoon}}^{\text{train}} \cup \mathcal{D}_{\text{adv}}^{\text{train}}$, where $\mathcal{D}_{\text{adv}}^{\text{train}}$ are adversarial scenarios created using our method applied to the original afternoon training data. We trained the adversary for $K = 15$ steps in Algorithm 1. We quantitatively compare the performance of all benchmark task models on mean task cost J and waypoint MSE on held-out test datasets for each condition, such as afternoon, morning, night (OoD), and synthetic test images ($\mathcal{D}_{\text{adv}}^{\text{test}}$).

2) *Quantitative results:* We now show that our TASK-DRIVEN scheme reduces the average task cost J compared to other task models. Fig. 4 (bottom left) shows the average task cost (Y-axis) for all the task models when evaluated on different test data scenarios (X-axis). On the afternoon and morning test scenarios, our TASK-DRIVEN scheme (red) performs on par with other task models. This is expected because all networks are trained on this data. Since the morning data is visually similar to the afternoon data, the task models perform similarly as well.

However, the key benefits of our approach are highlighted in the OoD night and synthetic adversarial test datasets. Our method automatically generates examples of challenging scenarios from the original afternoon training dataset and adds them to $\mathcal{D}_{\text{adv}}^{\text{train}}$, making the TASK-DRIVEN task model robust to OoD test datapoints as shown in the night and synthetic adversarial columns in Fig. 4. The DATA AUGMENTATION task model cannot help that much since it only creates single-step data augmentations that are often relevant only for the perception model but not necessarily for planning or control. Our TASK-DRIVEN scheme has 28.2% less average cost (Wilcoxon p-value of 0.0) for the night test dataset and 16.6% less average cost (Wilcoxon p-value of 0.0) for the

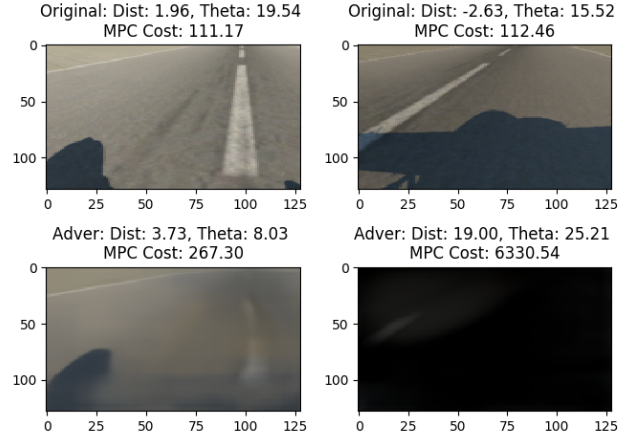


Fig. 5: X-Plane Synthetic Adversarial Scenarios: The top row contains images from the original dataset with the corresponding ground-truth label waypoint (distance to center-line and heading angle), as well as MPC task cost if this waypoint was correctly followed. The bottom row shows the corresponding adversarial scenario generated by our method. As expected, both the adversarial scenarios lead to higher MPC costs. On the left, the adversary learns to blur the runway center-line to emulate a foggy condition, while the right image emulates an OoD night scenario where only the center-line (top left) is faintly visible. Fig. 8 shows additional examples.

synthetic adversarial test dataset compared to standard data augmentation.

Figure 4 (bottom right) shows how our TASK-DRIVEN scheme achieves lower MPC task cost by predicting future waypoints w_F with lower MSE. While all methods perform similarly on the original test dataset $\mathcal{D}_{\text{afternoon}}^{\text{test}}$, the key gains of our scheme are on the night and synthetic adversarial test datasets. Specifically, the TASK-DRIVEN scheme has 54.7% less average cost (Wilcoxon p-value of 0.0) for the night test dataset and 42.6% less average cost (Wilcoxon p-value of 0.0) for the synthetic adversarial test dataset compared to standard data augmentation.

Qualitative Results: We now provide intuition for how our TASK-DRIVEN scheme outperforms standard benchmarks by illustrating challenging adversarial scenarios that we automatically synthesize in dataset $\mathcal{D}_{\text{adv}}^{\text{train}}$. Fig. 5 shows two scenarios where our adversarial training scheme makes it harder to detect the runway center-line. On the left of Fig. 5, the weather condition stays the same, but the centerline is blurred like in a foggy condition. On the right of Fig. 5, adversarial training changes the afternoon weather condition to night, which the ORIGINAL task model has never seen before. Naturally, this increases the task cost since the original task model mis-estimates the faintly visible center-line on the top left. As such, our scheme targetedly adds challenging scenarios to make the task model more robust.

It is important to note that the original renderer was trained on night training images so that the VAE can render a night scene in the first place. However, we strictly only trained the initial perception and planning models on the original afternoon training data. As such, they were never

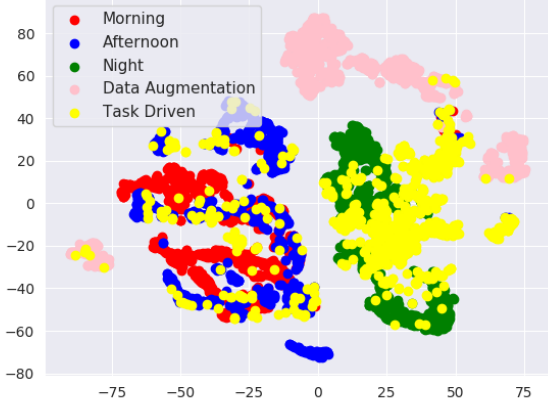


Fig. 6: X-Plane VAE Latent Space Visualization: We reduce the dimension of X-Plane test datasets to visualize their relative distance using the t-SNE method [17]. Recall that the perception module $z = \phi_{\text{perception}}(s; \theta_{\text{perc.}})$ takes an image s of the scene as input and outputs a latent representation z of the scene. Each dataset contains scenes s , and we visualize the corresponding latent variables z after passing the scenes through the perception module. The key takeaway is that the *Task Driven* scenes are very close to the OoD *Night* scenes, which explains why our *TASK DRIVEN* model performs so well on the OoD *Night* dataset. Additionally, the *Data Augmentation* scenes are not at all close to *Night* scenes, thus explaining why the *DATA AUGMENTATION* task model is not able to generalize to the OoD *Night* dataset. This visualization demonstrates how our task-driven method targettely generates synthetic scenarios to aid generalization on OoD data.

exposed to a single night (OoD) image. This scenario is practically motivated as, in reality, differentiable renderers have the ability to map a continuum of scene parameters v to scenes s , but we can only train the task model on a finite set of scenes v from a specific training distribution for cost-effective training. As such, our result illustrates that adversarial scenario generation can efficiently find and render scene parameters v that were not seen in the task model’s original training distribution. Naturally, for a fair comparison, all benchmarks used the same VAE renderer that was pre-trained initially and had frozen weights during adversarial scenario generation.

Finally, Fig. 6 shows the relative distance between different test datasets’ latent variables when projected in a 2D space using the t-SNE method [17]. Interestingly, our task-driven scheme is able to add synthetic data points (yellow) that emulate, and anticipate, the OoD night distribution. However, points added by standard data augmentation (pink) do not overlap much with the night data (green), explaining why the benchmark generalizes more poorly.

Limitations: In future work, we aim to develop theoretical generalization guarantees, at least for a linear adversary, simple generative model, and linear MPC.

V. CONCLUSION

This paper presents a principled method to automatically synthesize adversarial scenarios for vision-based robotic navigation and control tasks. Our first key insight is that

today’s adversarial example generation is largely limited to single-step inference and computer vision tasks, not multi-step planning tasks. As such, our key contribution is to compute the sensitivity of model-based control tasks to perception errors, which in turn guides how an adversary learns to generate hard-to-control visual examples. Moreover, by re-training on these synthesized adversarial examples, our method is able to generalize better to new test datasets than today’s task-agnostic data augmentation schemes. Our experiments on toy synthetic navigation problems and the photo-realistic X-Plane simulator demonstrate our approach can out-perform task-agnostic data augmentation by up to 28.2% on the out-of-distribution scenarios.

In future work, we plan to provide theoretical guarantees for an illustrative example with a linear adversary, simple linear renderer/scene generator, and linear MPC control problem. Moreover, we plan to compare how adversarial examples for single-step vision tasks differ from those generated by our synthesis approach for multi-step control problems. Finally, we plan to test the generalization ability of our approach on a small mobile robot operating in OoD lighting, weather, and terrain conditions.

REFERENCES

[1] X-plane 11. <https://www.x-plane.com/>.

[2] Y. Abeysirigoonawardena, F. Shkurti, and G. Dudek. Generating adversarial driving scenarios in high-fidelity simulators. In *2019 International Conference on Robotics and Automation (ICRA)*, pages 8271–8277. IEEE, 2019.

[3] A. Agrawal, B. Amos, S. Barratt, S. Boyd, S. Diamond, and Z. Kolter. Differentiable convex optimization layers. In *Advances in Neural Information Processing Systems*, 2019.

[4] A. Agrawal, S. Barratt, and S. Boyd. Learning convex optimization models. *arXiv preprint arXiv:2006.04248*, 2020.

[5] A. Agrawal, S. Barratt, S. Boyd, and B. Stellato. Learning convex optimization control policies. In *Learning for Dynamics and Control*, pages 361–373. PMLR, 2020.

[6] N. Akhtar and A. Mian. Threat of adversarial attacks on deep learning in computer vision: A survey. *Ieee Access*, 6:14410–14430, 2018.

[7] B. Amos, I. Jimenez, J. Sacks, B. Boots, and J. Z. Kolter. Differentiable mpc for end-to-end planning and control. In *Advances in Neural Information Processing Systems*, pages 8289–8300, 2018.

[8] F. Borrelli, A. Bemporad, and M. Morari. *Predictive control for linear and hybrid systems*. Cambridge University Press, 2017.

[9] A. Buslaev, V. I. Iglovikov, E. Khvedchenya, A. Parinov, M. Druzhinin, and A. A. Kalinin. Albumentations: Fast and flexible image augmentations. *Information*, 11(2), 2020.

[10] E. F. Camacho and C. B. Alba. *Model predictive control*. Springer Science & Business Media, 2013.

[11] K. Chaitanya, N. Karani, C. F. Baumgartner, A. Becker, O. Donati, and E. Konukoglu. Semi-supervised and task-driven data augmentation. In *International conference on information processing in medical imaging*, pages 29–41. Springer, 2019.

[12] T. Daniel and A. Tamar. Soft-intro vae: Analyzing and improving the introspective variational autoencoder. In *Proceedings of the IEEE/CVF Conference on Computer Vision and Pattern Recognition (CVPR)*, pages 4391–4400, June 2021.

[13] S. Feng, X. Yan, H. Sun, Y. Feng, and H. X. Liu. Intelligent driving intelligence test for autonomous vehicles with naturalistic and adversarial environment. *Nature communications*, 12(1):1–14, 2021.

[14] I. J. Goodfellow, J. Pouget-Abadie, M. Mirza, B. Xu, D. Warde-Farley, S. Ozair, A. Courville, and Y. Bengio. Generative adversarial networks, 2014.

[15] I. J. Goodfellow, J. Shlens, and C. Szegedy. Explaining and harnessing adversarial examples. *arXiv preprint arXiv:1412.6572*, 2014.

[16] D. Hendrycks, K. Zhao, S. Basart, J. Steinhardt, and D. Song. Natural adversarial examples. In *Proceedings of the IEEE/CVF Conference on Computer Vision and Pattern Recognition*, pages 15262–15271, 2021.

[17] G. E. Hinton and S. Roweis. Stochastic neighbor embedding. In S. Becker, S. Thrun, and K. Obermayer, editors, *Advances in Neural Information Processing Systems*, volume 15. MIT Press, 2003.

[18] H. Kato, D. Beker, M. Morariu, T. Ando, T. Matsuoka, W. Kehl, and A. Gaidon. Differentiable rendering: A survey. *arXiv preprint arXiv:2006.12057*, 2020.

[19] S. M. Katz, A. Corso, S. Chinchali, A. Elhafsi, A. Sharma, M. Pavone, and M. J. Kochenderfer. Nasa ulti aircraft taxi dataset, 2021. Stanford Research Data, <https://purl.stanford.edu/zz143mb4347>.

[20] S. M. Katz, A. L. Corso, C. A. Strong, and M. J. Kochenderfer. Verification of image-based neural network controllers using generative models. *arXiv preprint arXiv:2105.07091*, 2021.

[21] D. P. Kingma and M. Welling. Auto-encoding variational bayes, 2014.

[22] M. Lutter, S. Mannor, J. Peters, D. Fox, and A. Garg. Robust value iteration for continuous control tasks. *arXiv preprint arXiv:2105.12189*, 2021.

[23] A. Mandlekar, Y. Zhu, A. Garg, L. Fei-Fei, and S. Savarese. Adversarially robust policy learning: Active construction of physically-plausible perturbations. In *2017 IEEE/RSJ International Conference on Intelligent Robots and Systems (IROS)*, pages 3932–3939. IEEE, 2017.

[24] X. Pan, D. Seita, Y. Gao, and J. Canny. Risk averse robust adversarial reinforcement learning. In *2019 International Conference on Robotics and Automation (ICRA)*, pages 8522–8528. IEEE, 2019.

[25] K. Park, A. Mousavian, Y. Xiang, and D. Fox. Latentfusion: End-to-end differentiable reconstruction and rendering for unseen object pose estimation. In *Proceedings of the IEEE Conference on Computer Vision and Pattern Recognition*, 2020.

[26] L. Pinto, J. Davidson, R. Sukthankar, and A. Gupta. Robust adversarial reinforcement learning. In *International Conference on Machine Learning*, pages 2817–2826. PMLR, 2017.

[27] N. Ravi, J. Reizenstein, D. Novotny, T. Gordon, W. Lo, J. Johnson, and G. Gkioxari. Accelerating 3d deep learning with pytorch3d. *CoRR*, abs/2007.08501, 2020.

[28] O. Rybkin, K. Daniilidis, and S. Levine. Simple and effective vae training with calibrated decoders, 2021.

[29] A. Sharma, N. Azizan, and M. Pavone. Sketching curvature for efficient out-of-distribution detection for deep neural networks. *arXiv preprint arXiv:2102.12567*, 2021.

[30] J. Tobin, L. Biewald, R. Duan, M. Andrychowicz, A. Handa, V. Kumar, B. McGrew, A. Ray, J. Schneider, P. Welinder, et al. Domain randomization and generative models for robotic grasping. In *2018 IEEE/RSJ International Conference on Intelligent Robots and Systems (IROS)*, pages 3482–3489. IEEE, 2018.

[31] J. Tobin, R. Fong, A. Ray, J. Schneider, W. Zaremba, and P. Abbeel. Domain randomization for transferring deep neural networks from simulation to the real world. In *2017 IEEE/RSJ international conference on intelligent robots and systems (IROS)*, pages 23–30. IEEE, 2017.

[32] R. Volpi, H. Namkoong, O. Sener, J. Duchi, V. Murino, and S. Savarese. Generalizing to unseen domains via adversarial data augmentation. *arXiv preprint arXiv:1805.12018*, 2018.

[33] J. Wang, A. Pun, J. Tu, S. Manivasagam, A. Sadat, S. Casas, M. Ren, and R. Urtasun. Advsim: Generating safety-critical scenarios for self-driving vehicles. In *Proceedings of the IEEE/CVF Conference on Computer Vision and Pattern Recognition*, pages 9909–9918, 2021.

[34] M. Werling, J. Ziegler, S. Kammel, and S. Thrun. Optimal trajectory generation for dynamic street scenarios in a frenet frame. In *Proceedings - IEEE International Conference on Robotics and Automation*, pages 987 – 993, 06 2010.

[35] C. Xie, J. Wang, Z. Zhang, Y. Zhou, L. Xie, and A. Yuille. Adversarial examples for semantic segmentation and object detection. In *Proceedings of the IEEE International Conference on Computer Vision*, pages 1369–1378, 2017.

[36] S. Zakharov, W. Kehl, and S. Ilic. Deceptionnet: Network-driven domain randomization. In *Proceedings of the IEEE/CVF International Conference on Computer Vision*, pages 532–541, 2019.

APPENDIX

A. Experiment Details

Toy Experiment: In this experiment, the VAE Encoder is made up of 3 CNN layers with filter sizes of $[(3,3), (4,4), (5,5)]$, strides of $[1, 2, 2]$, and padding of $[1, 1, 2]$ respectively. Similarly, the decoder is made up of 3 CNN layers with filter sizes of $[(6,6), (6,6), (5,5)]$, strides of $[2, 2, 1]$, and padding of $[2, 2, 2]$ respectively. Rather than hand-tuning a desired weight between reconstruction error and KL divergence with a prior in the VAE loss, we use a σ -VAE [28] which allows for this tuning to happen automatically. We used a VAE with latent size of 20. The VAE is trained with the ADAM optimizer with a learning rate of $1e-3$. The encoder is used for the perception module $\phi_{\text{perception}}$ and the decoder is used for the differentiable rendering module ψ_{render} . Note that the encoder is re-trained after adversarial scenario generation.

Additionally, for the planning module, ϕ_{plan} is a NN consisting of three fully connected layers with ReLU activation functions with output sizes $[80, 60, 40]$ respectively. The planning module, ϕ_{plan} , is trained with the ADAM optimizer with a learning rate of $1e-3$. The robot's past waypoints w_P are of length $P = 10$ and the future waypoints w_F are of length $F = 20$. All the planning modules, ϕ_{plan} , were trained for 2000 epochs with early stopping. We experimented with multiple κ values (in loss Eq. 1) and finally used $\kappa = 30$ for the toy experiment. We found our results to be quite robust across a wide range of values κ .

X-Plane Experiment: In this experiment, we used a Soft-Intro VAE [12] in order to deal with realistic images. We used a Soft-Intro VAE with a latent size of 500. The Soft-Intro VAE is trained with the ADAM optimizer with a learning rate of $1e-3$. The encoder is used for the perception module $\phi_{\text{perception}}$ and the decoder is used for the differentiable rendering module ψ_{render} .

Additionally, for the planning module, ϕ_{plan} is a NN consisting of three fully connected layers with ReLU activation functions with output sizes $[256, 128, 2]$ respectively. The planning module, ϕ_{plan} , is trained with the ADAM optimizer with learning rate of $1e-3$. The robot's past waypoints w_P are of length $P = 4$ and the future waypoints w_F are of length $F = 1$. All the planning modules, ϕ_{plan} , were trained for 2000 epochs with early stopping. We experimented with multiple κ values (in loss eq. 1) and finally used $\kappa = 100$ for the X-Plane experiment.

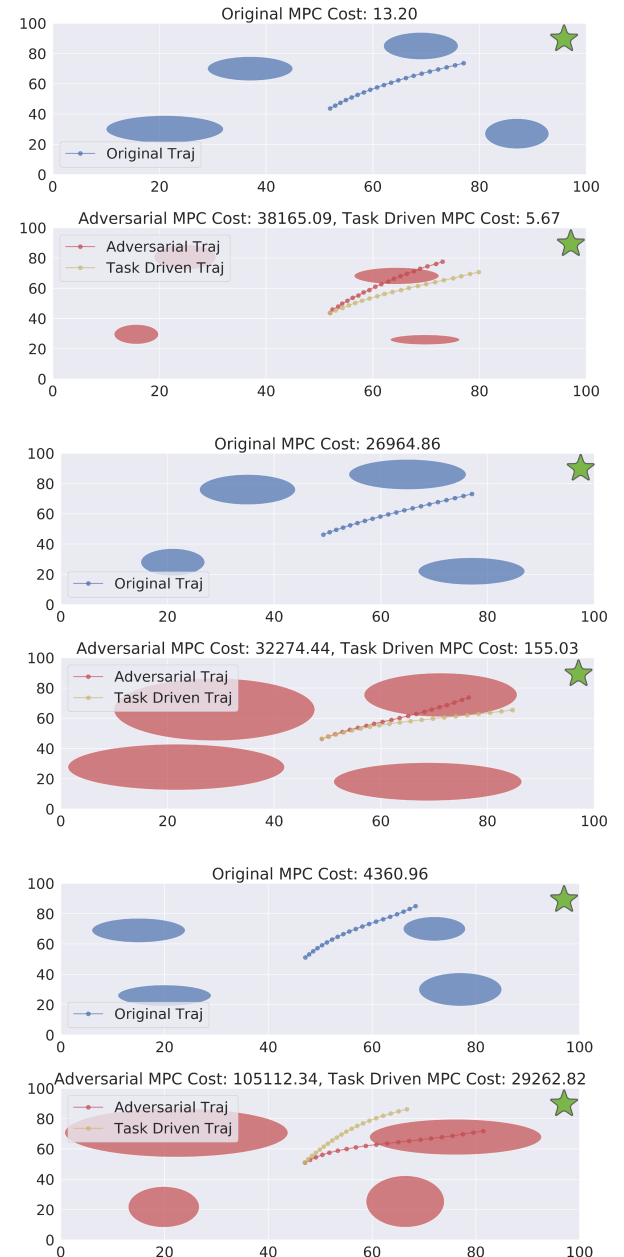


Fig. 7: Additional Synthesized Adversarial Scenarios for the Toy Motion Planning Experiment

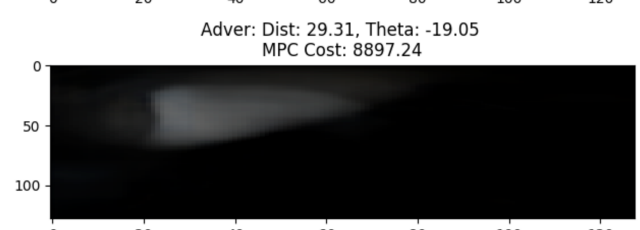
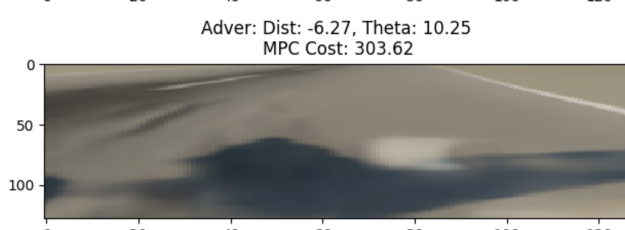
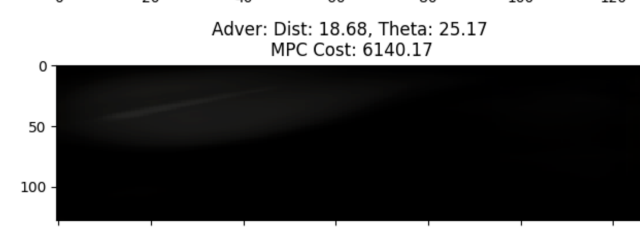
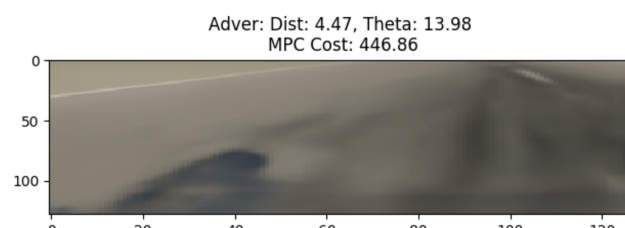
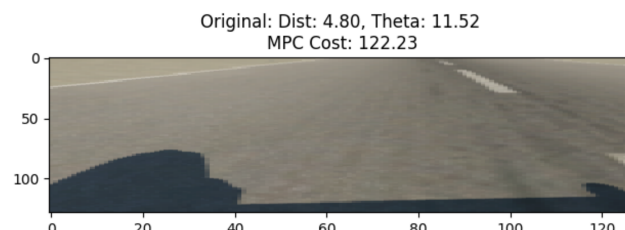
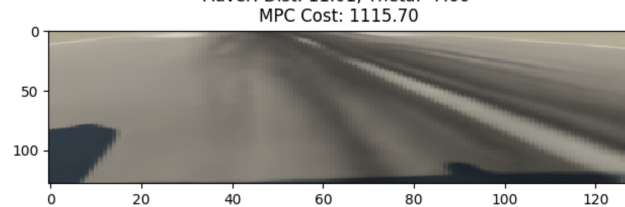
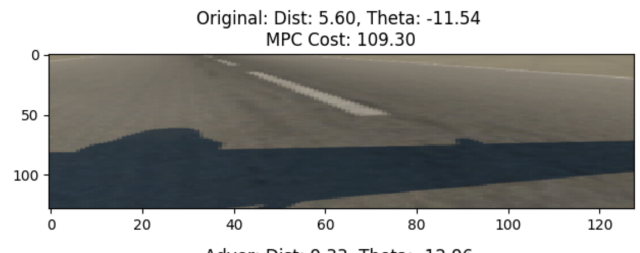
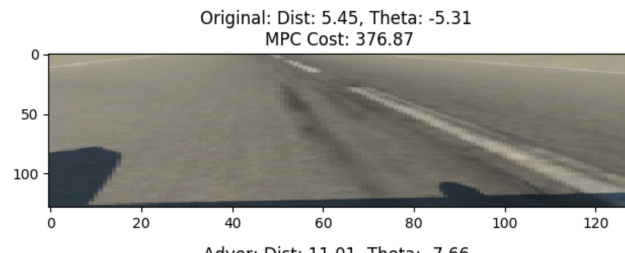


Fig. 8: Additional Synthesized Adversarial Scenarios for the X-plane Experiment